Indications of proton tunneling in the proton glass (betaine phosphate)$_{0.15}$(betaine phosphite)$_{0.85}$ from ENDOR and pulsed ESR studies

G. Völkel, H. Bauch, R. Böttcher, A. Pöppl, and H. Schäfer
Universität Leipzig, Fakultät für Physik und Geowissenschaften, D-04103 Leipzig, Germany

A. Klöpperpieper
Universität des Saarlandes, Fachbereich Physik, D-66123 Saarbrücken, Germany

(Received 18 November 1996)

The local proton order in the proton glass (betaine phosphate)$_{0.15}$ (betaine phosphite)$_{0.85}$ is studied by means of electron nuclear double-resonance and two-dimensional electron spin-echo envelope modulation (ESEEM) techniques. The experimental results allow very detailed comparisons with theoretical models such as the one-, and three-dimensional random-bond random-field (RBRF) Ising glass model. The attempt to describe the experimental behavior within the framework of the random-bond random-field (RBRF) Ising glass, which was worked out for deuteron glasses, suffers in conspicuous insufficiency at least at lower temperatures. Taking the influence of proton tunneling into account by using the stochastic model of a quantum RBRF Ising glass, the experimental results can fully be described. Furthermore, ESEEM experiments on a partially deuterated $BP_{0.15}BPI_{0.85}$ crystal confirm the different local polarization behavior in the protonated and deuterated hydrogen bonds in agreement with the model expectation. [S0163-1829(97)03618-7]

I. INTRODUCTION

In mixed crystals consisting of ferroelectric betaine phosphite (BPI) and antiferroelectric betaine phosphate (BP),[1] the frustrating interactions cause a glasslike order behavior[2] of the protons in the system of hydrogen bonds. Such materials belong to a class of orientational glasses that are designated as proton glasses. Model systems like spin glasses and orientational glasses are of special interest for the basic understanding of the glassy behavior of matter because for them theoretical model descriptions have been developed which allow comparisons with the experimental findings. Magnetic resonance proved to be one of the most appropriate techniques for the study of local proton or deuteron order and dynamics.[3] Deuteron glasses were carefully analyzed by deuteron nuclear magnetic resonance (NMR) where the local deuteron order is mirrored via the nuclear quadrupolar coupling. However, up to now there is no direct study of the proton order in a proton glass by H^1 NMR because with the chemical shift as the only interaction it is difficult to resolve local proton order. An interesting electron spin resonance (ESR) study of the local order-parameter distribution and the glass order parameter in the proton glass rubidium ammonium dihydrogen phosophate was achieved in an indirect way using substitutional Tl^{2+} ions at Rb sites as paramagnetic centers and probing the changes of the crystalline field at this site as a measure of the proton order at the PO_4 tetrahedra.[4]

In recent papers[5,6] we reported on the local proton order in the proton glass (betaine phosphate)$_{0.15}$(betaine phosphite)$_{0.85}$ studied by means of high-resolution ESR techniques such as electron nuclear double resonance (ENDOR) and electron spin echo envelope modulation (ESEEM) in a direct way via the proton hyperfine couplings. In this mixed crystal, the protons in the hydrogen bonds, linking the phosphite and phosphate groups to quasi-one-dimensional chains along the crystallographic b direction (see Fig. 1), show glassy behavior. We showed that the line shape of the ENDOR spectra of the protons in these hydrogen bonds is a direct measure of the local polarization distribution $W(p)$. The experimental determination of $W(p)$ allowed a very detailed comparison with theoretical models such as the one- and two-dimensional random-bond random-field (RBRF) Ising model.[7,8] The experimental Edwards-Anderson glass order parameter obtained as the second moment of $W(p)$ showed a temperature dependence

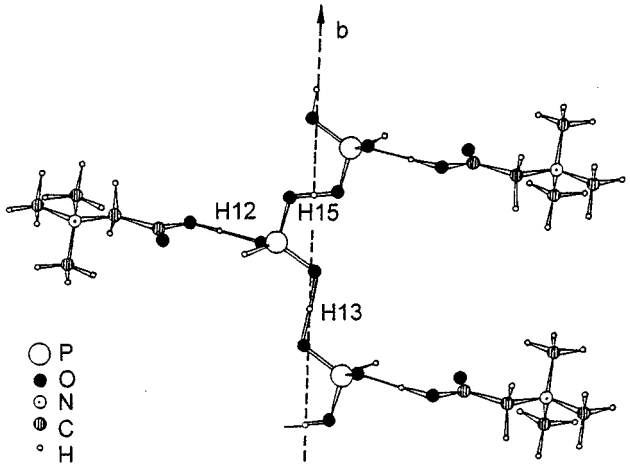

FIG. 1. Schematic drawing of the structure of BPI showing the chains of HPO_3 groups linked by hydrogen bonds with the protons H13 and H15. The betaine molecules are bound to the HPO_3 groups by one hydrogen bond (H12). In the mixed crystal, HPO_3 is partially substituted by HPO_4 to which the betaine is bound by two hydrogen bonds (H12 and H14).

which is characteristic for a proton glass with strong random fields. In order to reduce the number of fit parameters, the glass temperature $T_G = 30$ K was taken from dielectric results.[9] The unusually strong random fields, represented by the temperature $T_f = 95$ K, reflect the relatively strong distortions of the proton double minimum potentials in the hydrogen bonds adjacent to substitutional phosphate sites. The correspondence of the experimental data with the simulations improved considerably when a nonzero mean of the random bonds was introduced in the RBRF Ising model which indicates a smeared transition into a long-range ordered proton state at $T_c = 144$ K.

Though there is no doubt that the local proton order corresponds to the behavior expected for a proton glass there were still quantitative disagreements with the model simulations for lower temperatures, especially. The most striking difference with the model simulations is the fact that the experimental order-parameter distribution function takes its maximum at low temperatures not at $p = 1$ as the model predicts but at $p = 0.7$. Therefore, as an alternative procedure, in this paper we will take into consideration the influence of proton tunneling. Recently, theories for a quantum RBRF Ising glass have been published[10–12] which take into account proton tunneling. The aim of our paper is to show that using these theories a very convincing description of the experimental results succeeds. The tunneling energy $\Omega/k_B = 250$ K used as a fit parameter in our simulations is of the same order of magnitude as the tunneling energy $\Omega/k_B = 440$ K that explains the isotope shift[13] of the transition temperature into the ferroelectric phase of betaine phosphite of about 100 K due to deuteration. Furthermore, ESEEM experiments on a partially deuterated $BP_{0.15}BPI_{0.85}$ crystal confirm the different local polarization behavior in the protonated and deuterated hydrogen bonds in agreement with the model expectation. Taking into the considerations proton tunneling, the proton order in the BP_xBPI_{1-x} system can satisfactorily and unifiedly be described by the Ising model.

Recently a paper[14] was published reporting on the proton and deuteron glass dynamics in $Rb_{0.50}(NH_4)_{0.50}H_2PO_4$, $Rb_{0.58}(ND_4)_{0.42}D_2PO_4$, and $Rb_{0.68}(ND_4)_{0.32}D_2AsO_4$ studied by NMR spin-lattice relaxation measurements down to very low temperatures at the ^{87}Rb and O-D···O deuteron nuclei. The temperature independence of the relaxation rate at low temperatures is claimed to indicate the presence of phonon-assisted tunneling of the protons and deuterons within the hydrogen bonds resulting from the quantum glass character of these mixed compounds.

In Sec. II we will briefly quote some experimental details. In Sec. III a short outline of the theory will be given which is used in Sec. V to simulate and discuss the experimental results presented in Sec. IV.

II. EXPERIMENTAL

Mixed single crystals $BP_{0.15}BPI_{0.85}$ were grown by controlled evaporation from aqueous solution containing betaine with 15% H_3PO_3 and 85% H_3PO_4. The crystal growing procedure for deuterated mixed crystals $DBP_{0.15}DBPI_{0.85}$ was basically the same except that the parent materials were dissolved in D_2O. By analogy with the pure DBP (Ref. 15) and DBPI (Ref. 16) crystals one expects that only the protons H12, H13, H14, and H15 in the hydrogen bonds of the inorganic H_3PO_3 and H_3PO_4 groups (Fig. 1) should be replaced by deuterons in $DBP_{0.15}DBPI_{0.85}$. The degree of deuteration of the grown crystal amounts to about 85%. By γ irradiation of $BP_{0.15}BPI_{0.85}$ at room temperature PO_3^{2-} radicals were produced at PO_3 sites with a relative concentration of about 10^{-4}. Consequently, the proton order in the hydrogen-bridged phosphorus chains can only be probed at PO_3 but not at PO_4 sites. We proved by dielectric permittivity measurements of irradiated samples[17] that the dielectric behavior did not remarkably change. This result is understandable from the structural point of view as the proton missed at the radical is bonded to a lone orbital pair of the phosphorus atom that is not involved in the hydrogen bond system.

The ENDOR measurements were performed on the high-field ESR line of the ^{31}P hyperfine doublet.[18] The static magnetic field was applied parallel to the crystallographic ac plane forming an angle of 20° with the c direction such that the ENDOR line of proton H13 is not overlapped by other lines and that the individual line position of each proton is linearly related to its local polarization.[19] The measured ENDOR line shapes were analyzed by the Tikhonov regularization method[5,6] to deduce the experimental local polarization distribution $W(p)$. Additionally, we showed experimentally to be in the fast motional regime for the studied temperature range. Therefore, the line shape is proportional to $W(p)$ only. A very crucial point is the normalization of the ENDOR line scale with respect to the local order parameter p. In the Tikhonov regularization calculations this scaling was self-consistently done by taking the scaling unit $\omega_1 = \Delta\omega/2$ (see Sec. III) as an independent adjustable parameter. This scaling procedure is confirmed by the experimental line shapes themselves. The frequencies $(\omega_0 - \omega_1)/2\pi = 9.2$ MHz as the mean value of the low-frequency end of all the ENDOR lines corresponding to $p = 1$ and $\omega_0/2\pi = 12.1$ MHz as the central position of the ENDOR line at room temperature corresponding to $p = 0$ gives $\omega_1/2\pi = 2.9$ MHz in good agreement with the Tikhonov regularization result.

ESEEM investigations were performed on an ESP 380 Bruker FT ESR spectrometer. Two-dimensional (2D) ESEEM spectra were recorded using the hyperfine sublevel correlation spectroscopy (HYSCORE) sequence $(\pi/2 - \tau - \pi/2 - t_1 - \pi - t_2 - \pi/2 - \tau - \text{echo})$ with a pulse delay $\tau = 120$ ns or $\tau = 208$ ns to enhance proton or deuteron modulation, respectively. 256 steps in t_1 and t_2 were sampled with 16 ns (proton spectra) or 48 ns (deuteron spectra) dwell time. The echo decay was eliminated by a third-order polynomial base line correction of the experimental data set in both time domains. Before 2D Fourier transformation (FT) the data set was zero filled to 1024×1024 points. The 2D FT power spectra were calculated and presented as contour plots. All ESEEM spectra were recorded at the high-field signal of the PO_3^{2-} ESR doublet with the external magnetic field **B** directed parallel to the crystallographic bc plane with $\angle(\mathbf{B}, c) = 20°$ or $\angle(\mathbf{B}, c) = 45°$. For these orientations the ESR signals of the two magnetically nonequivalent PO_3^{2-} sites are well separated avoiding excitation of different crystallographic sites by the microwave pulses which might complicate the interpretation of the ESEEM spectra.

III. THEORY

Some years ago, theories of magnetic resonance line shape in proton glasses[12] were published where the effect of the tunneling motion of the protons in randomly mixed ferroelectric crystals was studied. Mean-field theory (MFT) was applied to the infinite-range model of an Ising spin glass with a transverse field describing the tunneling of a proton in the hydrogen bond. Two mechanisms have been discussed for the interplay of tunneling and thermally activated motion of the protons which both could be effective in real systems, depending on the temperature.[12] For the first mechanism it is assumed that the heat-bath coupling does not only cause random hopping of the proton from one site to another in its double-well potential, but also leads to incoherence in the tunneling process. The authors expect that this mechanism is dominant at higher temperatures. For the second mechanism predominating at low temperatures it is presupposed that only the hopping of the proton is aided by the stochastic forces of the heat-bath while tunneling remains uneffected and coherent. The interplay of tunneling and spin-glass-like ordering phenomena leads to characteristic features in the magnetic-resonance line shapes which permit discrimination between tunneling processes and classical thermally activated intrabond hopping across the potential barrier in proton glasses. This characteristic feature in the line shape does not show up only in the transition region from fast to slow motional regime,[12] manifesting itself in the appearance of an additional central line, but also in the fast motional regime because of the very special form of the order-parameter distribution function $W(p)$ due to proton tunneling. In the following, the main results of the theoretical approach for the simplified case of incoherent tunneling[12] are shortly outlined because this mechanism should be dominant in the experimentally studied temperature range.

It is assumed that the proton in an O-H$\cdots$O hydrogen bond moves in a double-well potential such that it spends most of its time at the bottom of either the left or the right well and very little in between. This is considered to be a two-level system described by the pseudospin variables $S^z = \pm 1/2$, which designate the left or right position of the proton in the double well. The proton with the nuclear spin $I=1/2$ will have the nuclear magnetic resonance frequencies ω_L and ω_R when it is on left and right side of the potential, respectively. The frequencies ω_L and ω_R result from transitions between the eigenstates of the nuclear-spin operator $I^z = \pm 1/2$ in the Hamiltonian for a proton in an isolated double well

$$H = \overline{\omega} I^z + \Delta\omega I^z, \tag{3.1}$$

where

$$\overline{\omega} = 1/2(\omega_L + \omega_R), \quad \Delta\omega = \omega_R - \omega_L . \tag{3.2}$$

Including now interwell interaction, random electric fields, and the possibility of tunneling between the two proton sites in a hydrogen bond, the Hamiltonian in Eq. (3.1) is to be extended by the terms of the interacting pseudospin system to

$$H = \overline{\omega}\sum_i I_i^z + \Delta\omega \sum_i I_i^z S_i^z - 1/2 \sum_{i,j} J_{ij} S_i^z S_j^z - \Omega \sum_i S_i^x - \sum_i f_i S_i^z . \tag{3.3}$$

Here, Ω is the tunneling frequency, J_{ij} is the infinite-ranged quenched random interaction between the pseudospins S_i^z, and f_i represents the random longitudinal field at site i. The quantities J_{ij} and f_i are supposed to be distributed independently one from another according to their respective Gaussian probability distributions:

$$P(J_{ij}) = \frac{1}{\sqrt{2\pi J^2}} \exp\left(- \frac{(J_{ij} - J_0)^2}{2J^2} \right), \tag{3.4}$$

$$P(f_i) = \frac{1}{\sqrt{2\pi\Delta}} \exp\left(- \frac{f_i^2}{2\Delta} \right). \tag{3.5}$$

The variance J of the random interactions determines the nominal glass temperature $T_0 \equiv J/4$, and often the variance of the random field Δ is expressed by the temperature $T_f \equiv \sqrt{\Delta}/2 = T_0\sqrt{\tilde{\Delta}}$ with $\tilde{\Delta} \equiv 4\Delta/J^2$. Though, in analogy to the nontunneling case[3,6] we take into consideration a nonzero mean of the random interactions $\langle J_{ij} \rangle = J_0 \neq 0$.

The pseudospin system is treated within the framework of a MFT of a quantum spin glass. The static effective single spin Hamiltonian can then be written as

$$H_0 = \Delta\omega I^z S^z - hS^z - \Omega S^x \tag{3.6}$$

with an effective field

$$h = h(\tilde{z}) = \frac{J}{2} \sqrt{q + \tilde{\Delta}}\, \tilde{z} + J_0 \overline{p} \tag{3.7}$$

acting on the pseudospin along the z axis due to a nonzero spin-glass order parameter q and a long-range polarization $\overline{p}$ where $\tilde{z}$ is a Gaussian noise field. The last equation differs from the original one in Ref. 11 in so far as we have included the term $J_0\overline{p}$ which refers to a nonzero mean of the quenched random interaction between the pseudospins. Thus the total field has the strength

$$h_0(\tilde{z}) = \sqrt{\Omega^2 + h(\tilde{z})^2}. \tag{3.8}$$

The mean-field equations for the local polarization p, its nonzero mean $\overline{p}$ and the spin-glass order parameter q are then obtained as

$$p(\tilde{z}) = r(\tilde{z}) \tanh\left(\frac{1}{2} \beta h_0(\tilde{z}) \right), \quad \beta = \frac{1}{k_B T}, \tag{3.9}$$

with

$$r(\tilde{z}) = \frac{h(\tilde{z})}{h_0(\tilde{z})}, \tag{3.9a}$$

$$\overline{p} = \frac{1}{\sqrt{2\pi}} \int_{-\infty}^{+\infty} \exp(-\tilde{z}^2/2) p(\tilde{z}) d\tilde{z} \tag{3.10}$$

and

$$q=\frac{1}{\sqrt{2\pi}}\int_{-\infty}^{+\infty}\exp(-\tilde{z}^2/2)p(\tilde{z})^2d\tilde{z}. \tag{3.11}$$

The local polarization distribution $W(p)$ has been calculated to take the form

$$W(p)=\frac{4\exp(-z_0^2/2)}{\beta J\sqrt{q+\tilde{\Delta}}}\left(r(z_0)^2+\frac{2\Omega^2}{\beta h(z_0)h_0(z_0)^2}\,p-p^2\right)^{-1}, \tag{3.12}$$

where $z_0=z_0(p)$ is the solution of Eq. (3.9) for a given p value. This equation includes now also the case of a nonzero average order parameter $\overline{p}$ because of Eq. (3.7). Consequently, we are able to model a system which can undergo a transition into a long-range ordered state but with considerable distribution of the local order parameter.

Until now the static properties of the system were only considered. In order to model its dynamics the system is assumed to be placed in contact with a heat bath. However, one expects the heat bath to induce not only classic thermal fluctuations but quantum fluctuations as well, leading to ''incoherence'' in tunneling. The usual way in the spirit of the kinetic Ising model of the Glauber type is to add to the static Hamiltonian in Eq. (3.6) coupling terms to the heat bath which are off diagonal in the representation where S^z is diagonal. When $\Omega\neq 0$, however, the appropriate quantization axis is not longer parallel to z but somewhere in-between the z and x directions. The simplest coupling to the heat bath is then assumed to be proportional to an operator that is strictly off diagonal in this new representation of the quantization axis of the quasispins. Using these assumptions, an individual line-shape function

$$I(\omega,p)=\frac{1}{4\pi}\,\frac{\lambda(\Delta\omega)^2[r(z_0)^2-p^2]}{\{\omega^2-1/4[r(z_0)\Delta\omega]^2\}^2+\lambda^2[\omega-(1/2)p\Delta\omega]^2} \tag{3.13}$$

is derived in the limit of a large ratio $J/\Delta\omega$ for a proton in a double-well potential which is at the same time subjected to thermal fluctuations with a relaxation rate λ and to incoherent tunneling.

The total line shape is given by

$$I(\omega)=\int_{-1}^{+1}dp\,W(p)I(\omega,p), \tag{3.14}$$

which reduces to

$$I(\omega)=\frac{1}{\Delta\omega/2}\,W\left(\frac{\omega}{\Delta\omega/2}\right) \tag{3.15}$$

in the fast motion limit. Consequently, in the fast motion regime, the order-parameter distribution function $W(p)$ is immediately given by the ENDOR line shape.

IV. RESULTS

The experimentally determined temperature dependence of the local order parameter distribution $W(p)$ of proton H13 is shown on the left side of Fig. 2. It was evaluated by means of the Tikhonov regularization technique from the ENDOR spectra.[5,6] The p scale is normalized as mentioned in Sec. II and the W scale such that $\int_1^{-1}W(p)dp=1$. The experimental $W(p)$ functions appear to be symmetric with respect to $p=0$. This is related to the special lattice site position of the protons H13 and H15 in the unit cell.

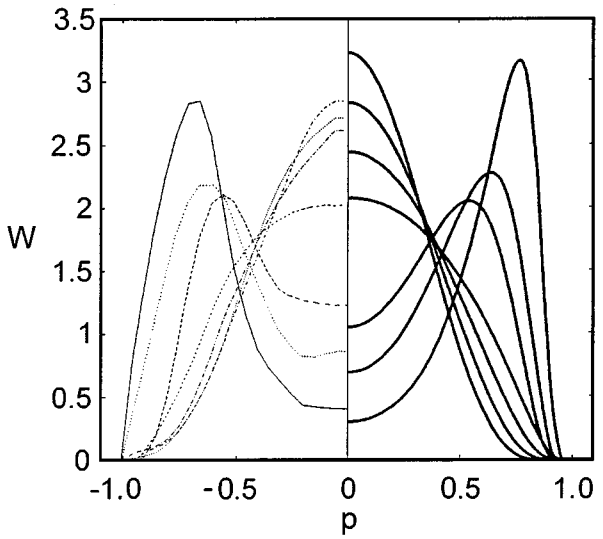

FIG. 2. Local order-parameter distribution function $W(p)$ of proton H13, attached to the PO_3^{2-} probe in $BP_{0.15}BPI_{0.85}$, for the temperatures 290 K (with highest W value at $p=0$), 250, 210, 170, 130, 120, and 90 K (with lowest W value at $p=0$). The experimental $W(p)$ distribution function is shown on left side. It was obtained from the ENDOR spectra taken at a magnetic-field direction in the crystallographic ac plane forming an angle of 20° with the c axis. The theoretical $W(p)$ distribution function according to the quantum Ising glass model is presented on right side. It was calculated using Eq. (3.12) and the parameter set given in the text. The $\tilde{\Delta}$ values were 10 for $T>144$ K and 3.4, 3.5, and 4.0 for $T<144$ K.

For simplicity, let us consider the isostructural BPI crystal. In the nonpolar phase of BPI, both protons are at lattice sites which are inversion centers with respect to the two neighbored phosphite groups. As a consequence, one would not obtain a linear relation between proton or deuteron polarization and NMR line shift in the polar phase with NMR techniques. However, in the case of ENDOR spectroscopy, the protons are detected via their hyperfine (hf) coupling to the attached PO_3^{2-} probe. The hf interaction does not show inversional symmetry with respect to the proton position. Therefore, a linear relation between the ENDOR line shift and the proton polarization p is not inconsistent with the local symmetry of the PO_3-H13 (H15) complex in BPI-type crystals. However, as the proton positions are symmetric in the nonpolar case with respect to the two neighbored phosphite groups labeled A and B, protons at equivalent sites with the same local polarization vector lead to ENDOR line shifts of opposite signs when the PO_3^{2-} probe is situated at A and B positions, respectively. The local symmetry relations for the proton sites in the mixed crystal are, in principle, similar.

These symmetry properties of the ENDOR spectra have to be taken into account in the case of nonzero long-range order of the proton system. The ENDOR spectrum consists then of two overlapping spectra for a defined sign of the averaged order parameter $\overline{p}$. Both spectra are inverted one to another

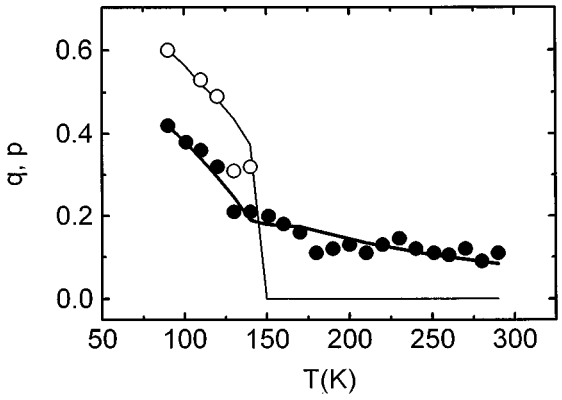

FIG. 3. Temperature dependence of the experimental long-range order parameter $\overline{p}$ (open circles) and the Edwards-Anderson glass order parameter q (full circles) of proton H13 attached to the PO_3^{2-} probe in $BP_{0.15}BPI_{0.85}$. The quantities $\overline{p}$ and q were obtained as the first and second moment of the experimental $W(p)$. The solid lines were calculated according to Eqs. (3.10) and (3.11) of the quantum Ising glass model using the parameters given in the text.

with respect to $p=0$. We showed in our former paper[6] that a nonzero average proton polarization $p\neq 0$ does exist for temperatures below $T_C=144$ K. Thus, the experimentally obtained symmetric $W(p)$ distribution shown in Fig. 2 has to be interpreted as consisting of two overlapping nonsymmetric parts

$$W(p)=W'(p)+W'(-p), \tag{4.1}$$

where the average order parameter of the protons is given by

$$\overline{p}=\int_{-1}^{+1} pW'(p)dp. \tag{4.2}$$

For that reason, $W(p)$ shown in Fig. 2 was empirically deconvoluted into $W'(p)$. This procedure allows us to calculate numerically the temperature dependence of the average proton order parameter $\overline{p}$ according to Eq. (4.2). The result is presented in Fig. 3. For the determination of the Edwards-Anderson glass order parameter q, there are no such problems. It can immediately be calculated from the experimental $W(p)$ distribution as q is defined by

$$q=\frac{1}{2}\int_{-1}^{+1} p^2W'(p)dp+\frac{1}{2}\int_{-1}^{+1} p^2W'(-p)dp$$
$$=\frac{1}{2}\int_{-1}^{+1} p^2W(p)dp. \tag{4.3}$$

The temperature dependence of the experimental glass order parameter q determined from the ENDOR spectra according to Eq. (4.3) is also shown in Fig. 3.

When tunneling is of importance for the protons but not for the deuterons, one can expect that even in a partially deuterated crystal the local polarizations of the protons and deuterons are different. Measurements of the local polarizations in a partially deuterated crystal have the big advantage that protons and deuterons are studied at the same physical conditions. We employed HYSCORE experiments in order to detect differences between the local polarization of the protons H13, H15 and the deuterons D13, D15 substituted at the same positions in a highly deuterated $DBP_{0.15}DBPI_{0.85}$ crystal. In the HYSCORE experiment of a $S=1/2$, $I=1/2$ spin system with small hyperfine coupling ($|A|<2\nu_I$) the correlations between the nuclear coherences of the two different electron spin (M_S) manifolds lead to cross peaks (ν_α,ν_β), (ν_β,ν_α) in the 2D spectra. Here ν_I is the nuclear Larmor frequency, A denotes the hyperfine coupling, and ν_α,ν_β are the nuclear transition frequencies in the two different M_S states. In the case of a $S=1/2$, $I=1$ spin system and small nuclear quadrupole interaction ν_Q ($|\nu_Q|\ll\nu_I,|A|$) as typical for deuteron nuclei, the nuclear quadrupole interaction gives rise to four nuclear transitions with the frequencies $\nu_{12}=\nu_\alpha+\nu_Q$, $\nu_{23}=\nu_\alpha-\nu_Q$, $\nu_{45}=\nu_\beta+\nu_Q$ and $\nu_{56}=\nu_\beta-\nu_Q$, where ν_Q is the nuclear quadrupole frequency. Thus, we would expect eight cross peaks (ν_{12},ν_{45}), (ν_{12},ν_{56}), (ν_{23},ν_{45}), (ν_{23},ν_{56}), (ν_{45},ν_{12}), (ν_{45},ν_{23}), (ν_{56},ν_{12}), and (ν_{56},ν_{23}) in the 2D spectrum. However, in the case of a $S=1/2$, $I=1$ spin system with small quadrupole interactions, these cross peaks are weighted by different intensity factors depending on the modulation depth parameter K and the pulse delay time τ in a similar manner as the modulation in the 1D four-pulse ESEEM experiment.[20] An analysis of these intensity factors reveals that the four cross peaks (ν_{12},ν_{45}), (ν_{23},ν_{56}), (ν_{45},ν_{12}), and (ν_{56},ν_{23}) have intensities proportional to K in the limit of small hyperfine couplings whereas the intensity of all other peaks are proportional to a higher power in K. As $K\ll 1$ usually holds in ESEEM experiments, the peaks (ν_{12},ν_{45}), (ν_{23},ν_{56}), (ν_{45},ν_{12}), and (ν_{56},ν_{23}) will dominate the 2D deuteron spectra in our case. A more detailed analysis of the cross-peak intensities in HYSCORE experiments in the limit of small nuclear quadrupole interactions will be given elsewhere.

Proton HYSCORE spectra recorded at room temperature for two different orientations are illustrated in Fig. 4. The assignment of the observed nuclear transition frequencies to the protons H13 and H15 are based on an angular dependence measured by the five-pulse sequence and a subsequent comparison with the hyperfine coupling tensors of H13 and H15 in $BP_{0.15}BPI_{0.85}$ given in a previous paper.[6] Cross-peak features were only observed in the first quadrant of the 2D plot as the condition $|A|<2\nu_1$ is valid for both protons H13 and H15.[6] The cross peaks of proton H13 at (18.07,14.71) MHz and (14.71,18.07) MHz are well separated from those of proton H15 at (18.43,13.55) MHz and (13.55,18.43) MHz for an orientation $\angle(\mathbf{B},c)=45°$ [Fig. 4(a)] due to different anisotropic hyperfine couplings of both protons for the selected orientation.[21] However, the cross peaks of both protons H13, H15 display a ridge-type shape indicating a strong inhomogeneous line broadening of the hyperfine signals which is caused by a distribution of the individual hyperfine coupling parameters.[22] These hyperfine coupling distributions reflect a variation of the local order parameter which can be observed in proton glass systems with strong random fields such as $BP_{1-x}BPI_x$ even far above the nominal glass transition temperature. For the other investigated orientation, $\angle(\mathbf{B},c)=20°$, the separation between the cross peaks of H13 and H15 is smaller and the correlation peaks merge into each other [Fig. 4(b)] due to the strong inhomogeneous broadening of the hyperfine signals.

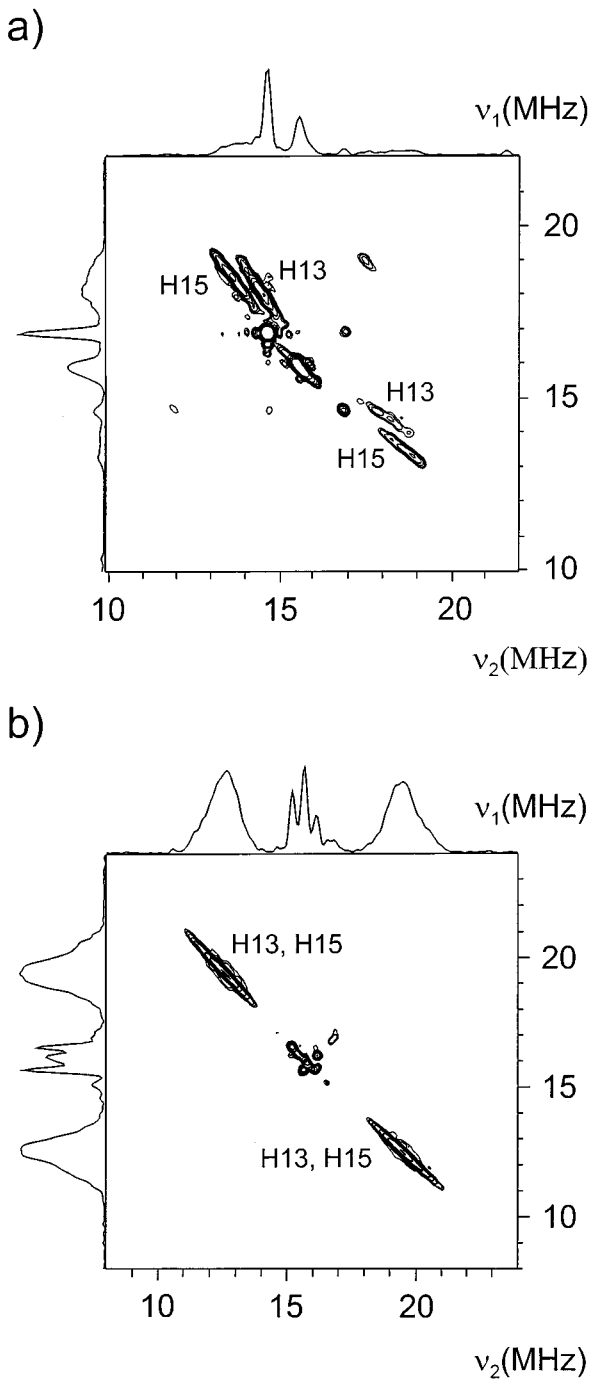

FIG. 4. HYSCORE spectra of protons H13 and H15 of γ-irradiated $DBP_{0.15}DBPI_{0.85}$ at 297 K. The spectra were obtained with **B** within the *bc* plane and (a) $\angle(\mathbf{B},c)=45°$ (b) $\angle(\mathbf{B},c)=20°$.

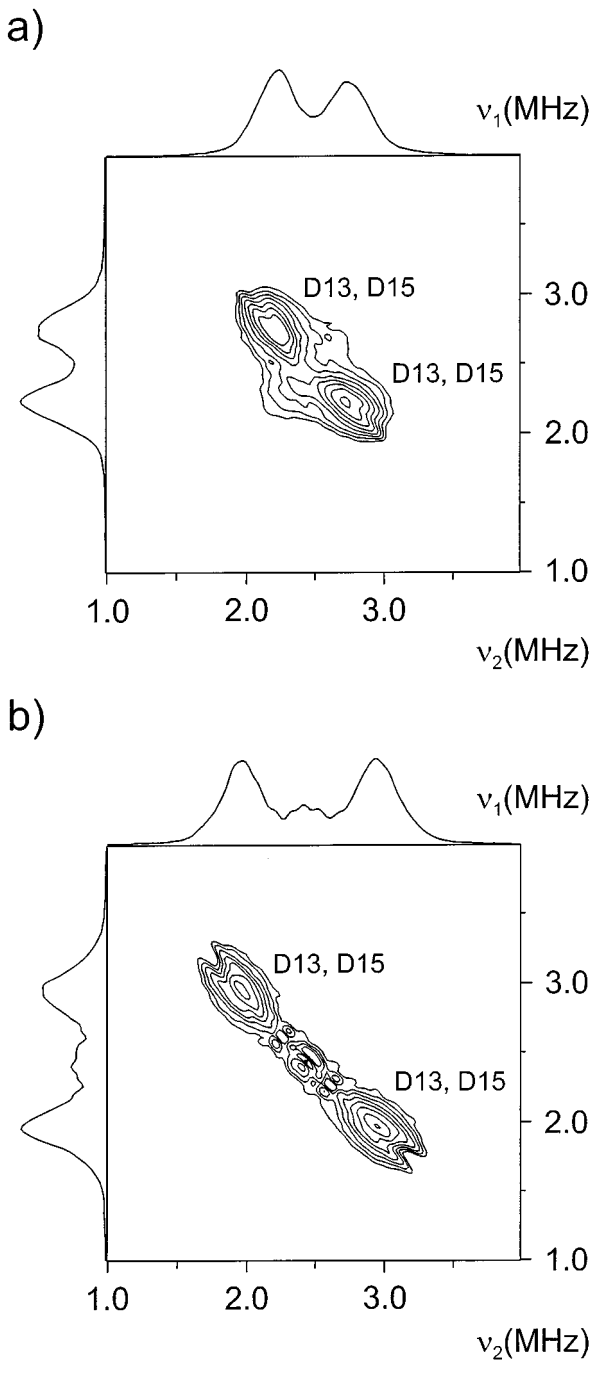

FIG. 5. HYSCORE spectra of deuteron nuclei D13 and D15 of γ-irradiated $DBP_{0.15}DBPI_{0.85}$ at 297 K. The spectra were obtained with **B** in the *bc* plane and (a) $\angle(\mathbf{B},c)=45°$, (b) $\angle(\mathbf{B},c)=20°$.

Deuteron HYSCORE spectra taken at the same orientations at room temperature are presented in Fig. 5. As in the case of protons, the assignment of the nuclear transition frequencies to the deuteron nuclei D13 and D15 is based on a measurement of their angular dependence using the five-pulse sequence. Again the line shape of the cross peaks of D13 and D15 reveals a remarkable inhomogeneous broadening of the corresponding nuclear transition frequencies which prevents a better resolved deuteron HYSCORE spectrum. The cross peaks of both deuteron nuclei could even not be resolved for $\angle(\mathbf{B},c)=45°$ as the nuclear quadrupole interaction of the deuteron nuclei leads to an additional line broadening of the correlation peaks. As for H13 and H15, the inhomogeneously broadened cross peaks of D13 and D15 likewise indicate a variation of the local order parameter of the deuterated hydrogen bonds.

Figure 6 shows a proton HYSCORE spectrum of γ-irradiated $DBP_{0.15}DBPI_{0.85}$ at $T=10$ K. The 2D spectrum reveals cross peaks of protons H13 and H15 in their mean close and far positions labeled by $H13_c$, $H13_f$, $H15_c$, and $H15_f$. Their nuclear transition frequencies have been deter-

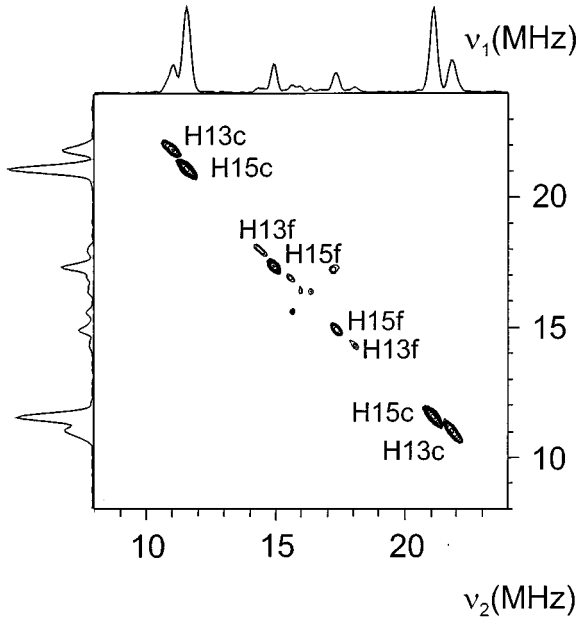

FIG. 6. Proton HYSCORE spectrum of γ-irradiated $DBP_{0.15}DBPI_{0.85}$ at 10 K. The marks c and f refer to the mean close and far positions of the protons H13 and H15 with respect to the PO_3^{2-} center. The spectra were obtained with **B** in the bc plane at $\angle(\mathbf{B},c)=20°$.

mined from the 2D plot in Fig. 6 and are summarized in Table I. Close and far positions of the protons H13 and H15 have also been observed in nondeuterated $BP_{0.15}BPI_{0.85}$ at low temperatures.[6] It was shown that there, these positions correspond to a local polarization of $|p|\approx 0.7$. Furthermore it is obvious from Fig. 6 that although the ridge-type shape of the cross peaks is not as pronounced as at $T=297$ K (Fig. 4) the cross-peak shape of the protons $H13_c$, $H13_f$, $H15_c$, and $H15_f$ still indicates some inhomogeneous broadening of the nuclear transition frequencies at $T=10$ K.

A deuteron HYSCORE spectrum at $T=10$ K is illustrated in Fig. 7(a). Eight intensive cross peaks are clearly resolved. We assign these peaks to the correlation peaks (ν_{12},ν_{45}), (ν_{23},ν_{56}), (ν_{45},ν_{12}), and (ν_{56},ν_{23}) of the mean close positions $D13_c$ and $D15_c$. An inspection of the central part of the deuteron 2D spectrum reveals the less intensive eight cross peaks of the mean far positions $D13_f$ and $D15_f$ [Fig. 7(b)]. The deuteron cross peaks show a circular shape which indicates the absence of any inhomogeneous broadening due to a variation of the local polarizations within the experimental error. The deuteron nuclear transition frequencies of $D13_c$, $D13_f$, $D15_c$, and $D15_f$ estimated from the HYSCORE spectrum are likewise summarized in Table I. In order to compare the frequency splittings $\Delta\nu_{\alpha/\beta}(D13)=\nu_{\alpha/\beta}(D13_c)-\nu_{\alpha/\beta}(D13_f)$ and $\Delta\nu_{\alpha/\beta}(D15)=\nu_{\alpha/\beta}(D15_c)-\nu_{\alpha/\beta}(D15_f)$ between the close and far positions of the deuteron nuclei with those of the protons H13 and H15, the deuteron nuclear transition frequencies without quadrupole splitting were calculated according to

$$\nu_{\alpha/\beta}=\frac{\nu_{12/45}+\nu_{23/56}}{2}. \tag{4.4}$$

The frequencies $\nu_{\alpha/\beta}$ of the deuteron nuclei are also included in Table I. It was shown in a previous ENDOR study on BPI that the frequency splittings $\Delta\nu_{\alpha/\beta}(H13)$ and $\Delta\nu_{\alpha/\beta}(H15)$ are linearly related to the local polarization p_H within the hydrogen bonds H13 and H15.[19] It is supposed that the same holds true for the deuterons also.

V. DISCUSSION

The comparison with the theory outlined above, leading to the determination of the model parameters, was done in the following way. In the first step, the self-consistent system of Eqs. (3.10) and (3.11) for the average proton order parameter $\overline{p}$ and the proton glass order parameter q was numerically solved, starting with parameters $J_0,\widetilde{J},\widetilde{\Delta}$ from the nontunneling case. The model parameters including Ω were varied such that the calculated glass order parameter q came close to the experimental one. In the next step, taking these parameters, the order-parameter distribution function given by Eq. (3.12) was calculated with $z_0=z_0(p)$ as the numerical solution of Eq. (3.9) for every considered value $-1\leqslant p\leqslant +1$. The distribution function $W(p)$ depends more sensitively on the model parameters as the integral value q. Therefore, the parameters were fine-tuned by adapting the theoretical $W(p)$ to the experimental one. In the last step, the theoretical values of q and $\overline{p}$ were calculated with this final parameter set. The results are illustrated in Figs. 2 and 3 as solid lines. The following parameters were obtained: $J_0/4k_B=200$ K, $\widetilde{J}/4k_B=30$ K, and $\Omega/k_B=250$ K. The parameter $\widetilde{\Delta}$ for the variance of the stochastic local field have to be adapted for every temperature under study separately. It

TABLE I. Nuclear transition frequencies $\nu_{ij}=\omega_{ij}/2\pi$ of the mean close and far positions of protons H13, H15 and deuteron nuclei D13 and D15 as determined from HYSCORE experiments at $T=10$ K.

	ν_{12}	ν_{23}	ν_{45}	ν_{56}	ν_α	ν_β
$H13_c$					11.07	21.83
$H13_f$					14.31	18.10
$H15_c$					11.54	21.10
$H15_f$					11.90	17.36
$D13_c$	1.709	1.607	3.438	3.343	1.658	3.391
$D13_f$	2.250	2.143	2.822	2.696	2.197	2.759
$D15_c$	1.719	1.719	3.337	2.255	1.719	3.296
$D15_f$	2.290	2.290	2.686	2.604	2.290	2.645

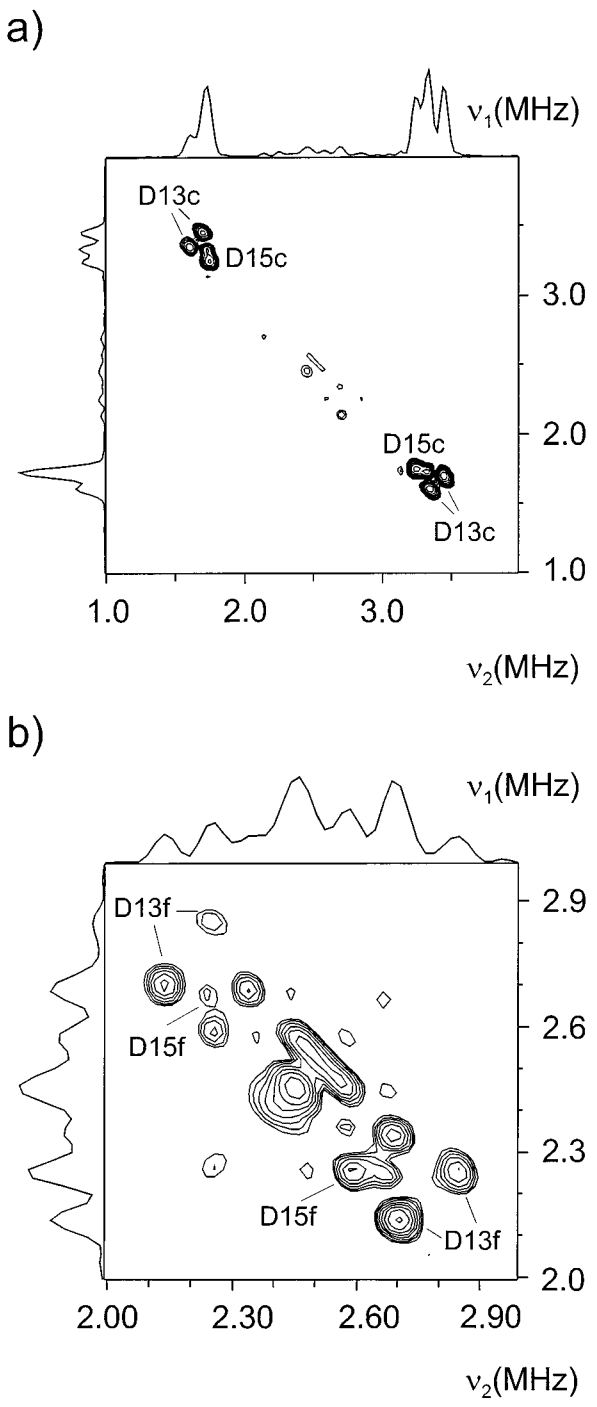

FIG. 7. Deuteron HYSCORE spectrum of γ-irradiated $DBP_{0.15}DBPI_{0.85}$ at 10 K. The marks c and f refer to the mean close and far positions of the deuteron nuclei D13 and D15 with respect to the PO_3^{2-} center. In (a) and (b) different contour levels and frequency scales are used as the cross peaks of $D13_f$ and $D15_f$ are less intense and closer to the Larmor frequency as those of $D13_c$ and $D15_c$. The spectra were obtained with **B** in the bc plane and $\angle(\mathbf{B},c)=20°$.

shows the following peculiarity: a temperature-independent value $\tilde{\Delta}=10$ is only estimated above $T_C=144$ K, whereas $\tilde{\Delta}$ drops steplikely down to a value $\tilde{\Delta}=2.5$ at T_C and rises up again with decreasing temperature to $\tilde{\Delta}=4$ at $T=90$ K. We assume that this peculiarity is related to the presence of long-range ordered domains. As already argued in our previous paper,[6] the temperature dependence of the stochastic fields below T_C might be attributed to a rearrangement of the local proton polarization with the growing up of domains which is not considered in the used theory. With the entrance into the long-range ordered phase, the nucleation of domains is starting in such a manner that their directions coincide with the mean direction of the local fields in this area. Consequently, the variance of the local fields is apparently reduced as many of the local-field directions coincide with the direction of the mean proton polarization. With growing up of the domain areas by lowering the temperature, more and more local-field positions are incorporated into the domain with conflicting directions which results in an increasing of the local-field variance. However, we have now to regard the presence of a nonzero mean polarization. As a consequence, a large number of local fields becomes nearly ineffective because their directions coincide with the direction of the mean polarization. Therefore, the variance of local fields in the ordered phase is distinctly lower than above T_C.

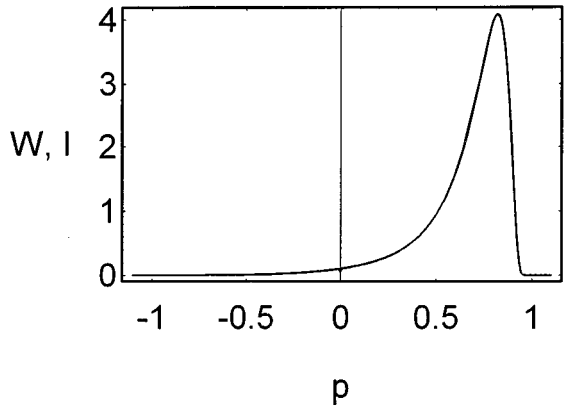

FIG. 8. Local order-parameter distribution W and ENDOR line shape I calculated for 30 K according to Eqs. (3.12), (3.13), and (3.14) with the parameters obtained at 90 K but using a relaxation rate $\lambda/\Delta\omega=1$. Both curves are identical on the normalized scale $2\omega/\Delta\omega=p$. No central line appears due to tunneling in the calculated ENDOR line shape I under the present conditions. The ENDOR line is still rather broad due to the remaining distribution of the local order parameter p.

It is worth mentioning that the appearance of an additional central line in the transition region from the fast to the slow motional regime is considered to be an unequivocal indication of proton tunneling.[12] However, such a central line cannot be expected in our case with the above parameter set as the following considerations show. The reasons for that are the strong local fields at the proton sites caused by both the large stochastic fields and the long-range order, as seen in Eq. (3.7). Using Eqs. (3.14), (3.12), and (3.13), the line shape $I(p)$ was calculated with the above parameter set but for $T=30$ K assuming a relaxation rate $\lambda/\Delta\omega=1$. The resulting line shape $I(p)$ is presented in Fig. 8 together with the order-parameter distribution function $W(p)$ on a normalized scale $2\omega/\Delta\omega=p$. No central line at all appears in the magnetic resonance line shape $I(p)$. Both $I(p)$ and $W(p)$ are practically identical.

In order to inspect whether the local polarization of a proton in the hydrogen bond is really smaller than that of an

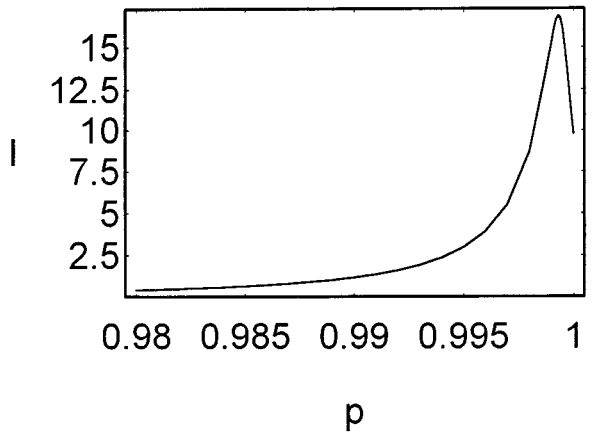

FIG. 9. ENDOR line shape I on the normalized scale $2\omega/\Delta\omega = p$ calculated for 30 K according to Eqs. (3.12), (3.13), and (3.14) with the parameters obtained at 90 K using a relaxation rate $\lambda/\Delta\omega = 1$ but putting $\Omega = 0$. Due to the absence of tunneling the ENDOR line appears very close to $p = 1$ and is very sharp because there is almost no distribution of p present anymore. Please note the strongly extended p scale.

substituted deuteron, additional ESEEM pulse experiments were performed on a 85% deuterated sample of $BP_{0.15}BPI_{0.85}$ at room temperature and $T = 10$ K. The static magnetic field was applied in directions where both the protons H13, H15 and deuterons D13, D15 were detectable and gave separate lines with a linear relation between ENDOR line position and local polarization. The room-temperature HYSCORE spectra of the protons and deuterons as well are definitely strongly inhomogeneously broadened as the ridge-type cross-peak shape[22] in Figs. 4 and 5 shows. Such a behavior is the expected one for a local order-parameter distribution as present in a proton or deuteron glass. The HYSCORE spectra of the protons H13, H15 and deuterons D13, D15 at 10 K, however, show a striking qualitatively different cross-peak shape. Whereas the deuteron cross peaks are of circular shape which is typical for a homogeneous line, the protons still show a ridge-type shape indicating an inhomogeneous broadening. This different behavior is also an indication for the appearance of proton tunneling as the model calculations show. We see in Fig. 8 that the calculated proton line at 30 K is considerably inhomogeneously broadened due to the still present local order-parameter distribution. The reason for this distribution at low temperatures is the influence of tunneling. Using the same parameter set but without tunneling ($\Omega = 0$), the resulting line shape is shown in Fig. 9. Now one obtains a very sharp line at $p = 1$ which is nearly perfectly homogeneous. This explains the circular cross-peak line shape of the deuterons for which tunneling is nearly not of importance.

As the investigation of the protons and deuterons was done at the same crystal sample, a direct comparison of their local polarizations is allowed. As already mentioned at the end of the former chapter, the local polarization p of the proton or deuteron in the hydrogen bond is proportional to the frequency splitting $\Delta\nu_{\alpha/\beta}$. When we assume that the factor of proportionality for protons and deuterons is also scaled with the quotient of their gyromagnetic ratios, the local polarizations of the deuterated hydrogen bonds D13

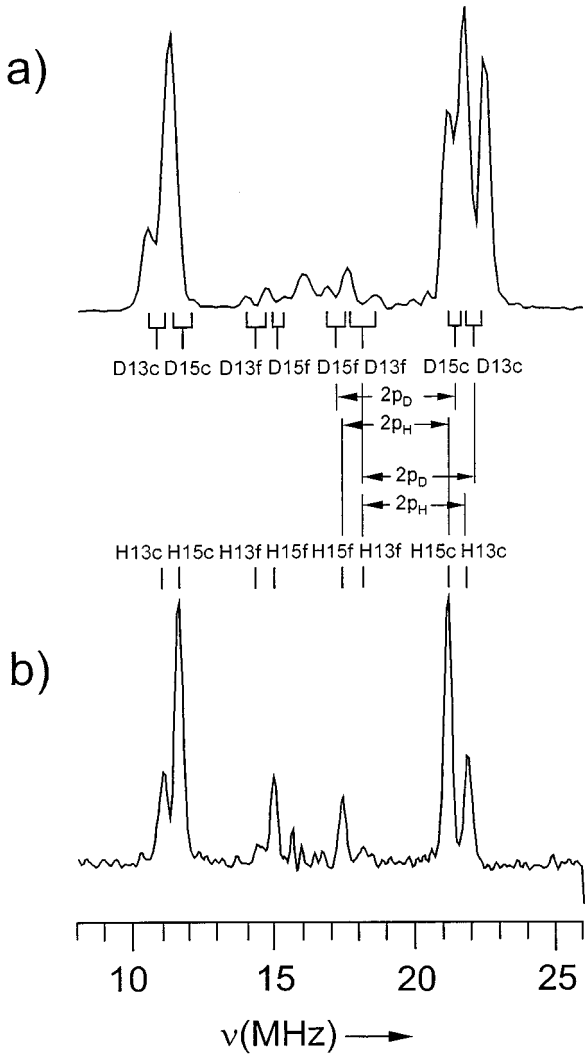

FIG. 10. Projections of the HYSCORE spectra at $T = 10$ K onto the ν_1 frequency axis. The deuteron spectrum is scaled by multiplying the deuteron frequencies by the quotient of the gyromagnetic ratios ν_H/ν_D: (a) projection of the deuteron HYSCORE spectrum, (b) projection of the proton HYSCORE spectrum. The spectra were obtained with $\mathbf{B}$ in the bc plane and $\angle(\mathbf{B},c) = 20°$.

and D15 can be compared with those of the nondeuterated bonds formed by protons H13 and H15 according to

$$p_H/p_D(H13) = \left| \frac{\nu_{\alpha/\beta}(H13_c) - \nu_{\alpha/\beta}(H13_f)}{\nu_{\alpha/\beta}(D13_c) - \nu_{\alpha/\beta}(D13_f)} \right|$$

and

$$p_H/p_D(H15) = \left| \frac{\nu_{\alpha/\beta}(H15_c) - \nu_{\alpha/\beta}(H15_f)}{\nu_{\alpha/\beta}(D15_c) - \nu_{\alpha/\beta}(D15_f)} \right|. \quad (5.1)$$

The quantities p_H and p_D denote the local polarizations of the O-H···O and O-D···O bonds, respectively.

The different local polarizations of the protonated and deuterated hydrogen bonds become obvious by a comparison of the projections of the proton and deuteron HYSCORE spectra onto the ν_1 frequency axis (Fig. 10). For this purpose the frequency scale of the deuteron spectrum was adapted to those of the proton spectrum by multiplying the deuteron

frequencies by the quotient of the gyromagnetic ratios ν_H/ν_D. The assignment of the deuteron frequencies to $D13_c$, $D15_c$, $D13_f$, and $D15_f$ was based on the interpretation of the deuteron 2D spectrum (Fig. 7). Figure 10 shows clearly that the splittings for the protons H13 and H15 between their mean close and far positions are smaller than those of the corresponding deuteron nuclei D13 and D15. On this renormalized frequency scale the line splittings $\Delta\nu_{\alpha/\beta}$ are a direct measure of the local proton and deuteron polarization as shown schematically on the high-frequency side of Fig. 10. Taking the experimental values from Table I we estimate using Eqs. (5.1) $p_H/p_D(\mathrm{H13}) = 0.91 \pm 0.04$ and $p_H/p_D(\mathrm{H15}) = 0.89 \pm 0.05$.

As one may assume that for deuterons the tunneling contribution is negligible, this experimental result obtained for the deuterated crystal confirms the findings for the protonated system. The normalized local proton polarization p remains smaller than one down to the lowest temperatures which underlines the importance of proton tunneling within the framework of the above applied model.

VI. CONCLUSIONS

High-resolution electron spin resonance (ESR) experiments on $(\text{betaine phosphate})_{0.15}(\text{betaine phosphite})_{0.85}$ provide a direct access to the study of the local proton polarization distribution and the glass order parameter in a proton glass. The attempt to describe the experimental behavior within the framework of the random-bond random-field (RBRF) Ising glass worked out for deuteron glasses suffers in conspicuous insufficiency at least at lower temperatures. Taking into consideration the influence of proton tunneling by using the model of a quantum RBRF Ising glass, the experimental results can fully be described when a tunneling energy $\Omega/k_B = 250$ K has been used. This value is of the same order of magnitude as the tunneling energy $\Omega_{T_C}/k_B = 440$ K that has to be taken in order to explain the shift of T_C from 220 K in protonated betaine phosphite to about 300 K in the deuterated compound. Therefore, we conclude quantum tunneling of the protons to be of relevant importance in betaine phosphate/phosphite proton glasses.

[1] J. Albers, A. Klöpperpieper, H. J. Rother, and S. Haussühl, Ferroelectrics **81**, 27 (1988).

[2] H. Ries, R. Böhmer, I. Fehst, and A. Loidl, Z. Phys. B **99**, 401 (1996).

[3] R. Blinc, Z. Naturforsch. **45a**, 313 (1989).

[4] R. Kind, R. Blinc, J. Dolinsek, N. Korner, B. Zalar, P. Cevc, N. S. Dalal, and J. DeLooze, Phys. Rev. B **43**, 2511 (1991).

[5] H. Schäfer and H. Bauch, Phys. Lett. A **199**, 93 (1995).

[6] H. Bauch, G. Völkel, R. Böttcher, A. Pöppl, H. Schäfer, J. Banys, and A. Klöpperpieper, Phys. Rev. B **54**, 9162 (1996).

[7] R. Pirc, B. Tadic, R. Blinc, and R. Kind, Phys. Rev. B **43**, 2501 (1991).

[8] M. Oresic and R. Pirc, Phys. Rev. B **47**, 2655 (1993).

[9] J. Banys, C. Klimm, G. Völkel, H. Bauch, and A. Klöpperpieper, Phys. Rev. B **50**, 16 751 (1994).

[10] T. K. Kopec, B. Tadic, R. Pirc, and R. Blinc, Z. Phys. B **78**, 493 (1990).

[11] B. Tadic, R. Pirc, and R. Blinc, Physica B **168**, 85 (1991).

[12] S. Dattagupta, B. Tadic, R. Pirc, and R. Blinc, Phys. Rev. B **44**, 4387 (1991); **47**, 8801 (1993).

[13] R. Blinc and B. Zeks, *Soft Modes in Ferroelectrics and Antiferroelectrics* (North-Holland, Amsterdam, 1974).

[14] J. Dolinsek, D. Arcon, B. Zalar, R. Pirc, R. Blinc, and R. Kind, Phys. Rev. B **54**, R6811 (1996).

[15] J. Albers, A. Klöpperpieper, H. J. Rother, and K. H. Ehses, Phys. Status Solidi A **74**, 553 (1982).

[16] H. Bauch, J. Banys, R. Böttcher, A. Pöppl, G. Völkel, and C. Klimm, Ferroelectrics **163**, 59 (1995).

[17] J. Banys, C. Klimm, G. Völkel, R. Böttcher, H. Bauch, and A. Klöpperpieper, J. Phys. Condens. Matter **8**, L245 (1996).

[18] A. Pöppl, G. Völkel, H. Metz, and A. Klöpperpieper, Phys. Status Solidi B **184**, 471 (1994).

[19] H. Bauch, R. Böttcher, and G. Völkel, Phys. Status Solidi B **179**, K41 (1993).

[20] A. M. Tyryshkin, S. A. Dikanov, and D. Goldfarb, J. Magn. Reson. A **105**, 271 (1993).

[21] A. Pöppl and L. Kevan, J. Phys. Chem. **100**, 3387 (1996).

[22] A. Pöppl, R. Böttcher, and G. Völkel, J. Magn. Reson. A **120**, 214 (1996).